Journal of Power Sources 195 (2010) 3097–3104

Contents lists available at ScienceDirect

Journal of Power Sources

journal homepage: www.elsevier.com/locate/jpowsour

$Cu_{1-x}Pd_x/CeO_2$-impregnated cermet anodes for direct oxidation of methane in $LaGaO_3$-electrolyte solid oxide fuel cells

Z.H. Bi, J.H. Zhu*

Department of Mechanical Engineering, Box 5014, Tennessee Technological University, 115 W 10th Street, Cookeville, TN 38505, USA

ARTICLE INFO

Article history:
Received 13 October 2009
Received in revised form
23 November 2009
Accepted 25 November 2009
Available online 2 December 2009

Keywords:
Solid oxide fuel cell
Composite anode
Impregnation
Cu–Pd alloy
Direct oxidation of methane

ABSTRACT

A series of ceramic–metal composite anodes containing 1.0 wt.% $Cu_{1-x}Pd_x$ alloys (where $x = 0$, 0.15, 0.25, 0.4, 0.5, 0.75 and 1.0) were prepared by impregnation of the respective metal salts and 5.0 wt.% CeO_2 into a porous $La_{0.4}Ce_{0.6}O_{2-\sigma}$ anode skeleton. The performance of these anodes was evaluated in both dry H_2 and CH_4 in the temperature range of 700–800 °C using the 300-μm thick $La_{0.8}Sr_{0.2}Ga_{0.83}Mg_{0.17}O_{3-\sigma}$ (LSGM) electrolyte-supported solid oxide fuel cells (SOFCs). The addition of Pd to Cu significantly increased the performance of the single cells in dry CH_4, with the cell maximum power density changed from 66 mW cm^{-2} for $Cu_{1.0}Pd_{0.0}$ to 345 mW cm^{-2} for $Cu_{0.0}Pd_{1.0}$ at 800 °C. In H_2, however, the performance improvement was not as significant compared to that in CH_4. In addition, carbon formation was greatly suppressed in the Cu–Pd alloy-impregnated anodes compared to that with pure Pd after exposure to dry CH_4 at 800 °C, which led to different performance stability behaviors for these cells operating with dry CH_4.

Published by Elsevier B.V.

1. Introduction

Direct oxidation of hydrocarbons in solid oxide fuel cells (SOFCs) has recently attracted tremendous interest as a promising process for portable generation of electrical energy. Various anode catalysts have been proposed, including ceria-based cermets [1], Sr-doped $LaCr_{0.5}Mn_{0.5}O_{3-\sigma}$ (LSCM) and $Sr_2MgMoO_{6-\sigma}$-based double perovskites [2,3], which were reported to be effective in preventing carbon formation and also to have good tolerance to sulfur when compared to conventional Ni-base anodes. For example, a SOFC with the CeO_2-based anode provided stable power generation from the fuels having 100–450 ppm of sulfur under various operation conditions, implying that natural gas and low-sulfur gasoline probably could be directly used as fuels for SOFCs without high desulfurization [4–8]. Unfortunately, the power densities of these cells with the oxide anodes were somewhat low due to the fact that the cermet anodes had insufficient conductivity and/or low activity toward hydrocarbon oxidation. Especially for methane, the reactivity of CH_4 to oxidation is extremely poor compared to other hydrocarbon fuels. Usually, Cu was added to improve the conductivity of the cermets because Cu is an excellent electronic conductor and yet a poor catalyst for coke formation; however, Cu is also a poor catalyst for C–H bond scission.

In order to obtain higher performance, one approach is the optimization of the structure of the cell with the Y_2O_3-stabilized ZrO_2 (YSZ) electrolyte, such as decreasing the thickness of the porous anode by using a thick $La_{0.3}Sr_{0.7}TiO_3$ current-collector layer or using cathode-supported configuration to decrease the ohmic resistance of the cell [9,10]. However, the fabrication process of the single cell likely needs to be simplified for commercial application while at the same time maintaining adequate performance. Another approach to improving the performance of the single cell with ceria-based cermet anodes is via alloying addition of a second metal into Cu to form a bimetallic alloy, such as Ni and Co [11–15]. For the Cu–Ni alloys, the addition of Ni to Cu significantly increased the performance of the cells for operation in H_2 and reduced coking in CH_4 compared to that with pure Ni, even though no change in performance with n-butane was observed. Unlike the Cu–Ni system, Cu–Co bimetallics exhibited a two-phase microstructure. It appears that when Cu covered the surface of most of the Co, the performance was improved for both H_2 and n-butane in the cells with a cermet anode with a Cu–Co alloy. The maximum power densities (MPDs) at 800 °C on the CeO_2 anode containing 20 wt.% $Cu_{0.5}Co_{0.5}$ were 570 and 360 mW cm^{-2} in dry H_2 and n-butane, respectively, compared to the values of only 420 and 300 mW cm^{-2} with 20 wt.% Cu, when the Cu (20 wt.%)–CeO_2 (10 wt.%)–YSZ (600 μm)/YSZ (60 μm)/$La_{0.8}Sr_{0.2}Mn_{3-\sigma}$ (LSM)–YSZ assembly was used [11]. Even with the thickness of the porous YSZ layer decreased to 400 μm, the single cell with the 80 wt.% Cu–20 wt.% Ni alloy–CeO_2 (10 wt.%)–YSZ (400 μm)/YSZ (60 μm)/LSM–YSZ assembly initially also showed very poor performance, only around 70 mW cm^{-2} at 0.5 V in CH_4 [12]. These results indicate that it is still needed to improve the activity of the anode with the impregnation of novel alloy catalysts for direct electrochemical oxidation of hydrocarbon fuels.

* Corresponding author. Tel.: +1 931 372 3186; fax: +1 931 372 6340.
E-mail address: jzhu@tntech.edu (J.H. Zhu).

0378-7753/$ – see front matter. Published by Elsevier B.V.
doi:10.1016/j.jpowsour.2009.11.111

Although ceria is one of the best oxidation catalysts among various oxides, its catalytic activity is not comparable to that of some metallic catalysts, particularly precious metals [16–18]. For example, the addition of dopant levels of Rh to a Sm_2O_3-doped CeO_2 (SDC) anode significantly improved the performance of the cell in CH_4 [18]. Recently, we have successfully replaced the porous (La,Sr)(Ga,Mg)$O_{3-\sigma}$ layer with a porous $La_{0.4}Ce_{0.6}O_{2-\sigma}$ (LDC) layer as a skeleton for metal catalyst impregnation on the LSGM electrolyte-supported single cell. The single cell with the porous LDC layer and lower loading of Cu (10 wt.%)–CeO_2 (5.0 wt.%) exhibited a higher performance than that with the porous LSGM layer and higher loading of Cu (20 wt.%)–CeO_2 (10 wt.%), due to the fact that LDC possesses a higher conductivity in a reducing atmosphere than LSGM [6,19]. The results also indicate that it is possible to decrease the metal catalyst loading to dopant levels to avoid catalyst sintering at cell operating temperatures.

In this paper, a series of composite anodes with the $Cu_{1-x}Pd_x$ (x = 0, 0.15, 0.25, 0.4, 0.5, 0.75 and 1.0) alloys were synthesized by co-impregnation technique. These composites were exposed to dry methane at 800 °C for 35 h to assess their carbon formation propensity. The LSGM electrolyte-supported cells with the porous LDC layer impregnated with the 1.0 wt.% $Cu_{1-x}Pd_x$ alloy and 5.0 wt.% CeO_2 as anode and $SrCo_{0.2}Fe_{0.8}O_{3-\sigma}$ as cathode were evaluated for direct electrochemical oxidation of dry CH_4 in the temperature range of 700–800 °C.

2. Experimental

2.1. Preparation of powder materials

Both the $La_{0.8}Sr_{0.2}Ga_{0.83}Mg_{0.17}O_{3-\sigma}$ (LSGM) and $La_{0.4}Ce_{0.6}O_{2-\sigma}$ (LDC) powders were synthesized by a conventional solid-state reaction procedure. La_2O_3 (Alfa Aesar, 99.99%), $SrCO_3$ (Alfa Aesar, 99.99%), Ga_2O_3 (Alfa Aesar, 99.999%), CeO_2 (Alfa Aesar, 99.99%) and MgO (Alfa Aesar, 99.99%) were used as starting materials. For synthesis of the LSGM powder, pre-treatment of La_2O_3 and MgO at 1000 °C for 10 h and $SrCO_3$ and Ga_2O_3 at 100 °C for 10 h was conducted in order to remove the hydroxides and carbonates. Stoichiometric amounts of pre-treated La_2O_3, $SrCO_3$, Ga_2O_3 and MgO were mixed evenly in an agate mortar, then pelletized and fired at 1250 °C for 5 h, followed by grinding with mortar and pestle. This process was repeated again. The LDC powder was synthesized similarly, with an intermediate firing temperature of 1400 °C. The $SrCo_{0.2}Fe_{0.8}O_{3-\delta}$ (SCF) cathode powder was prepared by the Pechini method, and was calcined at 800 °C for 5 h. All the powders were ball-milled for 0.5 h to reduce the particle size.

2.2. LDC–LSGM bilayer and cell fabrication

The bilayer structure with a dense LSGM electrolyte support and a porous LDC layer was fabricated by the uniaxial co-pressing approach. A layer of the LSGM powder with 0.5% PVB was initially placed in a metal die and pressed at 10 MPa; subsequently, a mixture of LDC and graphite pore formers was spread uniformly onto the LSGM layer. The bilayer was then pressed at 40 MPa to form a green body that was then fired for 4 h at 1450 °C in air. During the sintering process, the graphite pore formers were removed, leaving a porous LDC layer that was used as a skeleton for the Cu–Pd alloy and CeO_2 impregnation.

Single cells were fabricated as follows. First, the SCF cathode was fabricated by screen-printing on the LSGM electrolyte side of the LDC–LSGM bilayer with embedded Pt mesh and firing at 1100 °C for 0.5 h. The cathode area was 0.24 cm^2. CeO_2 was then loaded into the porous LDC layer by wet impregnation of an aqueous solution of $Ce(NO_3)_3$ (Alfa Aesar, 99.5%). The impregnated disc was then heated at 500 °C for 2 h to convert the nitrate into CeO_2. This process was then repeated until the CeO_2 loading in the LDC skeleton reached 5 wt.%, which was determined by measuring the weight change of the LDC skeleton before and after impregnation with a high-precision analytical balance. After achieving the required amount of CeO_2, the $Cu_{1-x}Pd_x$ alloy was introduced into the porous LDC layer by impregnation with a mixed $CuCl_2$ (Aldrich, 99.999%) and $PdCl_2$ (Aldrich, 99.9+%) solution in 10 wt.% HCl of the desired Cu and Pd atomic ratio, and then heated at 300 °C for 1 h. The impregnation/heat treatment cycle was carried out repeatedly in order to get the proper loading of the $Cu_{1-x}Pd_x$ alloys. After reduction in 95% Ar + 5% H_2 at 800 °C for 5 h, the weight percentage of the metal catalyst in the LDC skeleton was around 1.0 wt.%. The chemical compositions of the resulting $Cu_{1-x}Pd_x$ alloys attained from solutions were verified via lattice parameter measurement with X-ray diffraction (XRD). Au mesh with several separate dots of Au paste was used as the anode-side current collector.

2.3. Evaluation of the $Cu_{1-x}Pd_x$ alloys and single cells

To determine the effect of the Cu–Pd alloy composition on the propensity of the impregnated anodes to form carbon deposits in dry CH_4, a series of co-fired LSGM–porous LDC bilayers impregnated with 5.0 wt.% CeO_2 and 1.0 wt.% $Cu_{1-x}Pd_x$ alloys with different x values were reduced in 5% H_2 + 95% Ar at 800 °C for 5 h, and then exposed to flowing CH_4 at 800 °C for 35 h. These impregnated bilayers were identical to the cells used in fuel cell testing, except that the SCF cathode was not attached on the LSGM side. Carbon formation was assessed by both visual examination and measurement of the weight change of the anode as a function of the exposure time in CH_4 at 800 °C.

The single cell was sealed onto an Al_2O_3 tube with Pyrex glass. The assembled test cell was placed in a vertical furnace with the cathode exposed to ambient air and the anode to dry H_2 and CH_4 at a flow rate of 40 ml min^{-1}. The single-cell tests were carried out using an electrochemical interface (Solartron 1287) with a LabVIEW program at 700, 750 and 800 °C in H_2. The fuel was then switched to dry CH_4; once the single cell open-circuit voltage (OCV) in CH_4 was relatively stable, the single-cell performance was measured at the three different temperatures. The electrochemical impedance spectra (EIS) of the single cells were measured with the electrochemical interface and a frequency response analyzer (Solartron 1260) under the open-circuit voltage (OCV) condition. The frequency range was from 1 MHz to 0.01 Hz and the AC amplitude was 10 mV. For some cells, the performance stability in CH_4 at 800 °C was also determined at a cell voltage of 0.5 V.

After cell testing, some cells were fractured manually and the cross-sections of the tested cells were examined using a scanning electron microscope (SEM, FEI XL30) attached with an energy-dispersive spectroscope (EDS).

3. Results and discussion

3.1. Typical microstructure of the single cells

Typical cross-sectional views of the fractured cells after cell testing in CH_4 are shown in Fig. 1. According to Fig. 1(a), the dense LSGM electrolyte and the porous LDC layers were uniform and well-sintered. The thickness of the LSGM electrolyte, porous LDC anode layer and screen-printed SCF cathode layer was ~300, ~100 and ~20 μm, respectively.

According to Fig. 1(a), no cross-membrane cracks or open pores were present in the electrolyte. In addition to the numerous fine pores, a small number of large-sized pores were also observed in the LDC skeleton layer; however, the total porosity in the LDC layer was

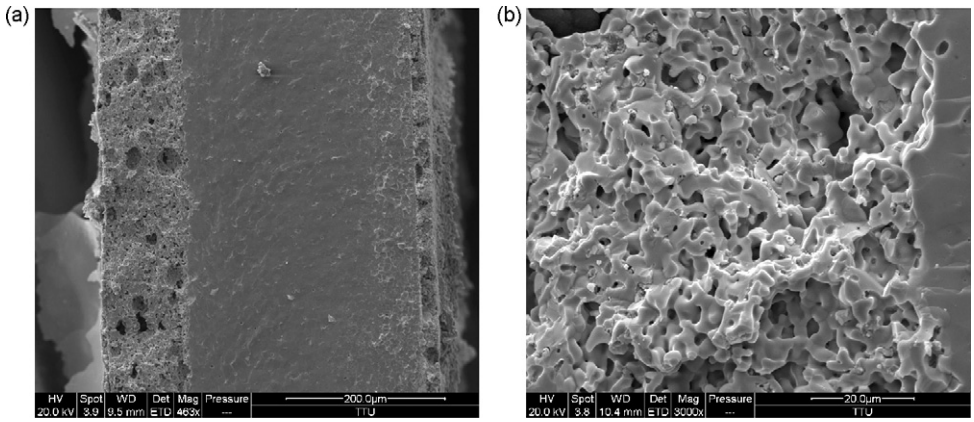

Fig. 1. Cross-sectional images of the fractured cell after operation in CH_4: (a) overall view of the cell and (b) the microstructure of the LDC anode impregnated with 1 wt.% Cu and 5 wt.% CeO_2.

only about 27% due to co-firing with the LSGM electrolyte at high temperature. This level of porosity is sufficient for the relatively low loadings of CeO_2 and metal catalysts used in this study, as no gas diffusion polarization was observed for a similar anode in our previous work [6]. Low porosity might be beneficial as it improves the conductivity of the anode. From Fig. 1(b), a small amount of metal and CeO_2 particles were dispersed on the large LDC grains due to the low loading of metal and CeO_2 (i.e. 1.0 and 5 wt.%, respectively).

3.2. Characterization of the $Cu_{1-x}Pd_x$ alloys

Impregnation with a mixed solution of $CuCl_2$ and $PdCl_2$ resulted in the formation of the solid-solution $Cu_{1-x}Pd_x$ alloys after reduction in 5% H_2 + 95% Ar at 800 °C for 5 h. According to the XRD results, all the Cu–Pd alloys exhibited a face-centered cubic structure at room temperature upon cooling down from the reducing temperature; the variation of the lattice parameter for the Cu–Pd alloys with the molar fraction of Pd ions in the impregnation solution is shown in Fig. 2. Since the lattice parameter of the Cu–Pd solid solution was also almost a linear function of the Pd content [20], the x value in the $Cu_{1-x}Pd_x$ alloy was very close to the molar fraction of Pd in the impregnation solution, indicating that the desired alloy compositions were achieved in the impregnated Cu–Pd alloys.

The chemical composition of the Cu–Pd alloy catalysts had a significant effect on the propensity of the impregnated anodes to coke. The weight change of the bilayer impregnated with various $Cu_{1-x}Pd_x$ alloys is plotted in Fig. 3 after different times of exposure to dry CH_4 at 800 °C. For the bilayers with $x \leq 0.4$ in $Cu_{1-x}Pd_x$, the weight remained essentially constant upon exposure to CH_4 at 800 °C for 35 h. However, as x increased to larger than 0.4, noticeable weight increase was observed, which became more severe as x increased from 0.5 to 1. Apparently, the amount of carbon deposited on the Pd-impregnated bilayer was the highest, which seemed to increase continuously with the exposure time. However, for the $Cu_{0.5}Pd_{0.5}$- and $Cu_{0.25}Pd_{0.75}$-impregnated bilayers, the amount of carbon deposited in the anode approached a relatively stable value after 15-h exposure.

Consistent with these observations, a small amount of carbon was visible only on the bilayer impregnated with Pd, even though the overall color of all the discs changed to black after exposure in CH_4 for 35 h. With the introduction of Cu into Pd to form the $Cu_{1-x}Pd_x$ alloys, carbon deposition was significantly suppressed compared to pure Pd, which might be due to the enrichment of Cu on the surface of the $Cu_{1-x}Pd_x$ alloys, similar to the Cu–Ni alloy system [12].

3.3. Electrochemical performance of the anodes impregnated with the $Cu_{1-x}Pd_x$ alloys

Fig. 4(a) and (b) shows the voltage and power density as a function of current density for the cell impregnated with pure Cu as

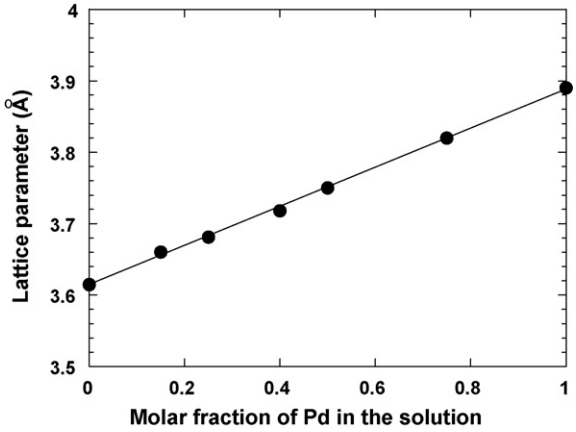

Fig. 2. Variation in lattice parameter of the Cu–Pd alloy with molar fraction of Pd in the Cu–Pd impregnation solution.

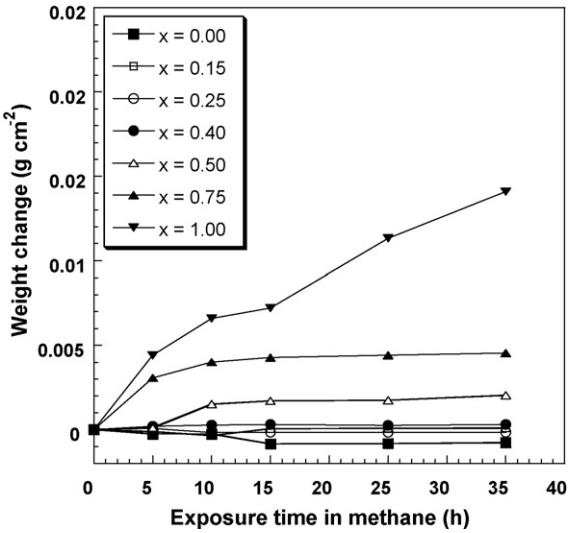

Fig. 3. Weight change as a function of exposure time to flowing CH_4 at 800 °C for the 1.0 wt.% $Cu_{1-x}Pd_x$/5.0 wt.% CeO_2-impregnated LDC–LSGM bilayer discs. These LDC–LSGM bilayer discs were identical to the cells used in the single cell testing and were reduced in 5% H_2 + 95% Ar at 800 °C for 5 h prior to exposure to CH_4.

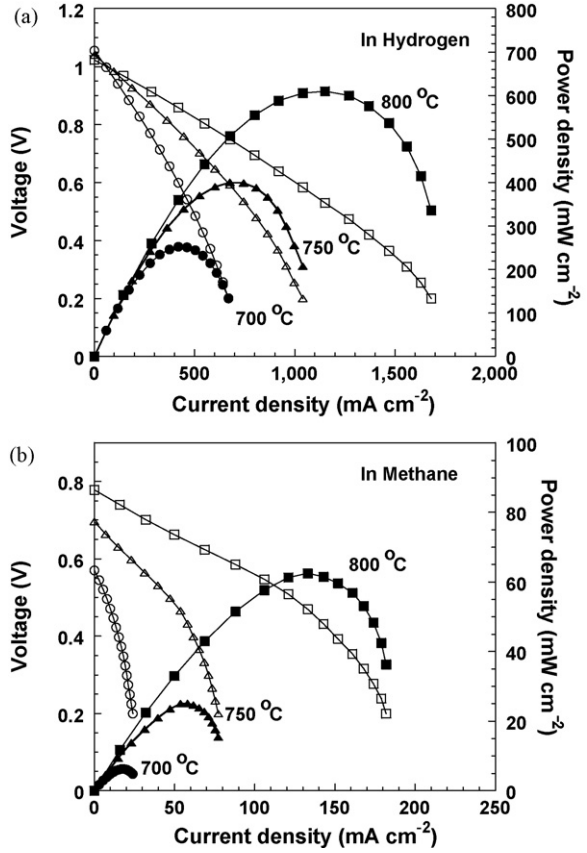

Fig. 4. Voltage and power density as a function of current density for the single cell impregnated with pure Cu as the anode at various temperatures: (a) in H_2 and (b) in CH_4.

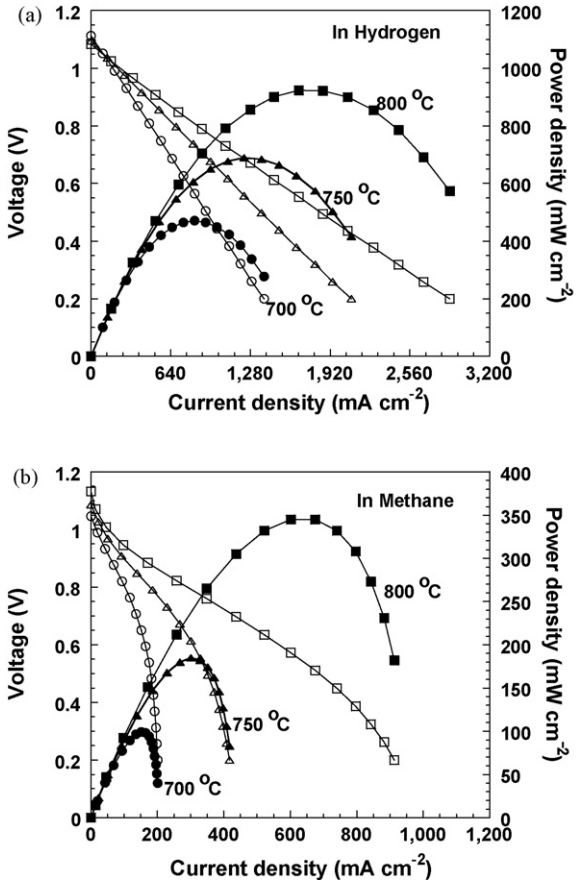

Fig. 5. Voltage and power density as a function of current density for the single cell impregnated with pure Pd as the anode at various temperatures: (a) in H_2 and (b) in CH_4.

the anode at different temperatures in dry H_2 and CH_4, respectively. The MPDs for the cell with the Cu–CeO_2–LDC anode in H_2 were 610, 400 and 252 mW cm^{-2} at 800, 750 and 700 °C, respectively. The performance was slightly lower than that of the single cell with the 10 wt.% Cu–5.0 wt.% CeO_2 anode reported in our previous work [6], due to the decreased loading of Cu from 10 to 1.0 wt.%. With the impregnation of 1.0 wt.% Cu the electronic conductivity of the anode is not expected to increase drastically as that impregnated with 10 wt.% Cu. Similarly, the MPDs for the cell in CH_4 also decreased to 62, 25 and 6 mW cm^{-2} at 800, 750 and 700 °C, respectively. These MPD values are close to those for the 5.0 wt.% Cu-containing cell with a 12-μm porous YSZ/50-μm dense YSZ/300-μm YSZ–LSF ($La_{0.8}Sr_{0.2}FeO_{3-\sigma}$) combination, as reported by Gross et al. [21].

When pure Cu was replaced with pure Pd, the performance of the single cell increased significantly. Fig. 5(a) and (b) represents the voltage and power density as a function of current density for the cell with a Pd–CeO_2–LDC anode at different temperatures in dry H_2 and CH_4, respectively. The MPDs for this cell in H_2 was 923, 689 and 471 mW cm^{-2} at 800, 750 and 700 °C, respectively. Thus, an improvement of 50–80% in performance of the single cell in H_2 was obtained by impregnation with pure Pd over that with pure Cu. The most significant benefit with the impregnation of Pd was observed in CH_4 with the MPDs of the single cell reaching 345, 185 and 100 mW cm^{-2} at 800, 750 and 700 °C, respectively. There is also an increase in the OCV in CH_4. The OCV for the cell with the Pd–CeO_2–LDC anode was approximately 1.13, 1.09 and 1.05 V at 800, 750 and 700 °C, respectively. Comparing Fig. 4 with Fig. 5, it can be seen that the OCV of the cell impregnated with 1.0 wt.% Cu was much lower than that of the cell impregnated with 1.0 wt.% Pd.

Fig. 6 summarizes the MPDs of the single cells with the different $Cu_{1-x}Pd_x$ anodes in H_2 and CH_4 at 800 °C. Clearly, the performance of single cells increased with the Pd content in the $Cu_{1-x}Pd_x$ alloys. This is especially true in CH_4 where the performance of the single cells was improved almost linearly with the increasing Pd content in $Cu_{1-x}Pd_x$. In H_2, however, when the Pd content was higher than 40%, the single cells attained a relatively constant MPD of ~900 mW cm^{-2} at 800 °C. The results indicate that the addition of Pd affected the performance of the single cells in H_2 much less than that in CH_4, as hydrogen oxidizes much more readily than

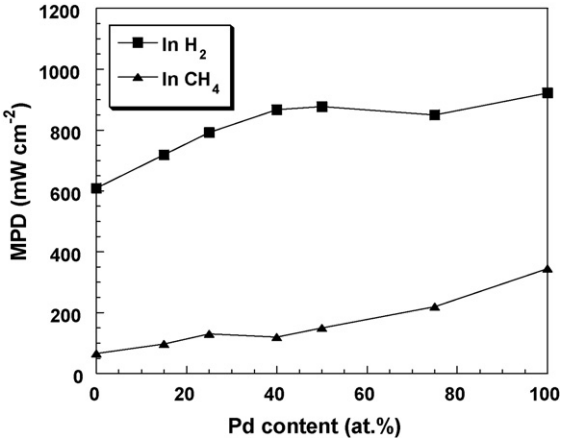

Fig. 6. Maximum power densities of the single cells using H_2 and CH_4 as fuel at 800 °C as a function of the Pd content in the $Cu_{1-x}Pd_x$ alloys.

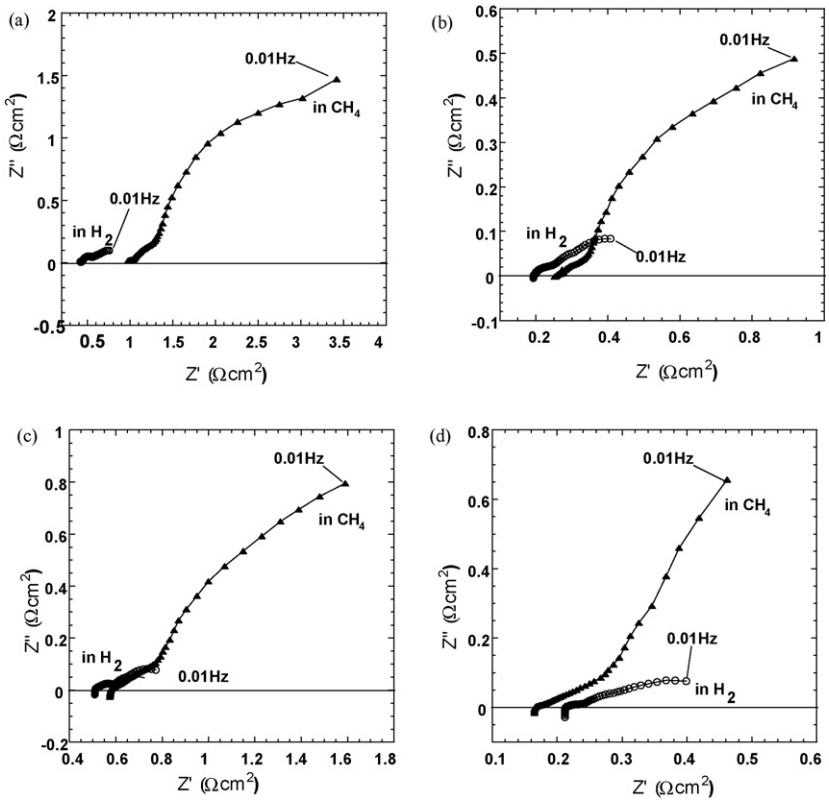

Fig. 7. Impedance spectra of the single cells in dry H_2 and CH_4 at different temperatures: (a) $Cu_{0.5}Pd_{0.5}$-impregnated anode in H_2 and CH_4 at 700 °C; (b) $Cu_{0.5}Pd_{0.5}$-impregnated anode in H_2 and CH_4 at 800 °C; (c) Pd-impregnated anode in H_2 and CH_4 at 700 °C; (d) Pd-impregnated anode in H_2 and CH_4 at 800 °C.

CH_4. Pd is the most commonly used catalyst for complete oxidation of methane and supported Pd has also been found to be the most promising catalyst for the oxidation of methane [22–24]. The variations in activity for methane oxidation under different reaction conditions have been correlated with the corresponding changes in the particle size and morphology of catalyst, the composition of the reaction mixture in the anode, and the nature of the active sites. An increase of Pd content in the $Cu_{1-x}Pd_x$ alloys is likely to lead to an increase in the number of surface active sites, which could improve the surface reaction of methane on the $Cu_{1-x}Pd_x$ alloy-containing anodes.

The electrochemical impedance spectra of the single cells with different anodes at 700 and 800 °C were measured under the OCV conditions in dry H_2 and CH_4, respectively. Fig. 7(a) and (b) is the impedance spectra of the single cell with the $Cu_{0.5}Pd_{0.5}$-impregnated anode in H_2 and CH_4 at 700 and 800 °C, respectively. The total ohmic resistance of the single cell from the connecting wire, electrolyte, electrode and the electrolyte–electrode interfaces was determined by the high-frequency intercept of the impedance spectrum. Mainly two frequency-dependent arcs with characteristic frequencies at around 4 Hz and 0.01 Hz were observed in the impedance spectra for both H_2 and CH_4. For comparison, the impedance spectra of the single cell with Pd-impregnated anode with H_2 and CH_4 at 700 and 800 °C, are also shown in Fig. 7(c) and (d), respectively. From Fig. 7(a)–(d), the total cell resistance as determined by the low-frequency intercept in the impedance spectrum of the single cells in H_2 was much lower than that of the single cell in CH_4, consistent with the performance of the single cells in H_2 and CH_4. According to the previous data reported by Ye et al. [25], the reduction in electrode impedance with Pd impregnation is primarily on the impedance at low frequencies likely associated with the methane oxidation reaction. The second arc with characteristic frequency at the low-frequency region can probably be attributed to the anode process, because the cathode condition remained the same. The ohmic resistance obtained from the high-frequency intercept of the impedance spectrum was increased from 0.422 to 0.968 Ω cm^2 when H_2 was changed to CH_4 for the single cell with the $Cu_{0.5}Pd_{0.5}$-impregnated anode at 700 °C. A similar change was also observed in the cell with the Pd-impregnated anode from 0.510 to 0.577 Ω cm^2 at 700 °C. However, the increase in cell ohmic resistance for the pure Pd-impregnated cell is much lower than that for the $Cu_{0.5}Pd_{0.5}$-impregnated cell. After the operating temperature was increased to 800 °C, the ohmic resistance of the single cell with a $Cu_{0.5}Pd_{0.5}$-impregnated anode in H_2 was still lower than that in CH_4. For the single cell with a Pd-impregnated anode, however, the ohmic resistance decreased to only 0.165 Ω cm^2 in CH_4, which is lower than 0.214 Ω cm^2 for the single cell in the H_2 at 800 °C from Fig. 7(d).

In order to clarify the effect of Pd content in the $Cu_{1-x}Pd_x$ alloys on the ohmic resistance of the single cells with the $Cu_{1-x}Pd_x$-impregnated anodes in CH_4, the ohmic resistance of the single cells in H_2 and CH_4 at 700 °C is plotted in Fig. 8. The ohmic resistance of the single cells in H_2 was similar, indicating that the thickness of the electrolyte and the porous LDC layer were uniform and reproducible. The ohmic resistance of all the single cells increased when the fuel was changed from H_2 to CH_4 at 700 °C. The increasing ohmic resistance was probably due to the fact that the conductivity of LDC in dry CH_4 was lower than that in H_2, as the total conductivity of the doped CeO_2 is strongly dependent on the oxygen partial pressure (P_{O_2}) in the environment [26,27]. This is in contrast to the ohmic resistance of the single cell with the Pt–CeO_2-impregnated anode being independent of fuel reported by McIntosh et al. [18]. There are probably two reasons for such different behaviors. Firstly, the skeleton that used in McIntosh's study was Y_2O_3-stabilized ZrO_2 (YSZ), the conductivity of which is independent of P_{O_2}; secondly, a carbonaceous layer was deposited by exposing the anode to flowing,

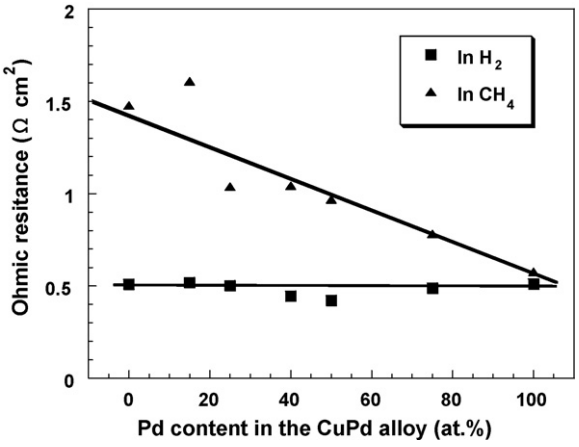

Fig. 8. The ohmic resistance of the single cells with the $Cu_{1-x}Pd_x$-impregnated anodes in H_2 and CH_4 at 700 °C as a function of the Pd content in the $Cu_{1-x}Pd_x$ alloys.

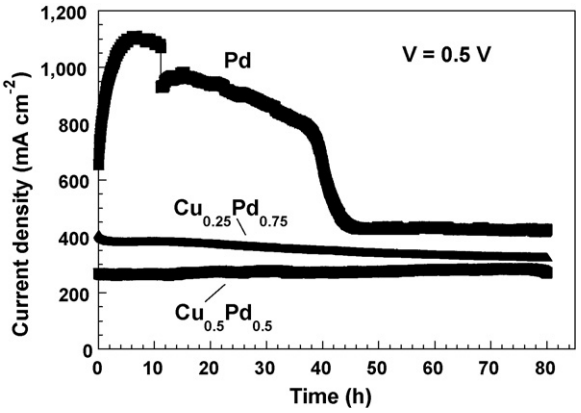

Fig. 9. Variation in current density with time for the cells with the $Cu_{0.5}Pd_{0.5}$-, $Cu_{0.25}Pd_{0.75}$- and $Cu_{0.0}Pd_{1.0}$-impregnated anodes operating at a constant voltage of 0.5 V at 800 °C in dry CH_4.

dry n-butane at 700 °C for 4 h before the cell was tested. Such exposure treatment produced polyaromatic compounds at a coverage of nearly 4 wt.% in the anode, which led to the electronic conductivity of the anode being independent of P_{O_2} [28]. However, only 1.0 wt.% metal was impregnated into the porous LDC layer in this work; therefore, the conductivity of the anode could be dominated by the LDC. When the anode was exposed in CH_4, the carbon started to form in the anode which led to improvement in its electronic conductivity. More carbon was deposited on the $Cu_{1-x}Pd_x$ anodes with a higher Pd content, which resulted in lowering the ohmic resistance of the single cell, consistent with the weight change of the bilayer exposed to CH_4, as shown in Fig. 3. From Fig. 7(d), the ohmic resistance of the single cell in CH_4 with the Pd-impregnated anode was lower than that in H_2 at 800 °C, most likely due to the formation of more carbon in the Pd-impregnated anode at this temperature.

3.4. Comparison in performance stability of single cells with the $Cu_{1-x}Pd_x$ anodes

To determine whether the performance stability of the single cells was affected by the carbon deposition in the $Cu_{1-x}Pd_x$ anodes, the single cells with Pd-, $Cu_{0.5}Pd_{0.5}$- and $Cu_{0.75}Pd_{0.75}$-impregnated anodes were selected for evaluation in CH_4 at 800 °C for around 80 h, due to their relatively higher output power. Because of the small electrode size, the utilization of the fuel was less than 1% at reasonable flow rates, implying that the H_2O:CH_4 ratio in the anode compartment was negligible. The cell potential was fixed at 0.5 V and the current density was measured as a function of operation time, with the data shown in Fig. 9. The current density of the single cell with a Pd-impregnated anode increased rapidly from 654 to 1110 mA cm^{-2} in 5 h, followed by a gradual decrease to 764 mA cm^{-2} in the next 32 h. A precipitous drop in current density from 764 to 420 mA cm^{-2} within 7 h was then observed. In the final 40 h of operation, the single cell performance remained essentially unchanged.

One model reported in the previous works [12,29] might be adopted to explain the change of current density in the different periods for our Pd-impregnated cell in CH_4. In that model, the metal particles (e.g. Cu or Cu–Ni) are mainly an electronic conductor rather than a catalyst in the three-phase boundary region of the metal–CeO_2–YSZ anode. The model suggests that some metal or alloy particles are not connected to the outside circuit and cannot assist in the removal of the electrons. Therefore, the entire region under these isolated metal particles is ineffective in the electrochemical reaction without charge transportation. With carbon formation, some isolated metal particles could become electronically connected to the outside circuit, which should lead to more of the anode surface being involved in the electrochemical reaction. In our Pd-impregnated anode, however, Pd is a good electronic conductor as well as a highly active catalyst. It is perceived that some isolated Pd particles were also ineffective for electrochemical reaction since they also lacked charge transportation. With a small amount of carbon formed at the anode, some isolated Pd particles become active, leading to the performance of the single cell increasing rapidly in the beginning. During further cell testing, more carbon is formed, leading to some Pd particles being covered and therefore ineffective. As a result, the performance of the single cell starts to drop slowly in this stage. In the third period, a rapid drop was observed in the stability testing, possibly due to some Pd particles being completely covered by the carbon deposits as well as some pores being fully blocked by the carbon deposits such that the electrochemical reaction is impaired due to these active sites lacking fuel. However, in the final stage, the current density of the single cell was still stable at 418 mA cm^{-2} for an additional 40 h, likely due to the low Pd loading (1.0 wt.%) in the anode. Such low Pd loading might cause some areas free of the Pd particles in the three-phase region to be unaffected by carbon formation, where the methane was electrochemically oxidized by CeO_2 rather than by Pd.

Compared to the single cell with a Pd-impregnated anode, the current densities of the single cells with $Cu_{0.25}Pd_{0.75}$ or $Cu_{0.5}Pd_{0.5}$-impregnated anodes were relatively stable throughout the stability testing. This result is likely due to the fact that the carbon formation decreased significantly by introducing Cu into Pd to form the $Cu_{1-x}Pd_x$ alloys, as shown earlier. With limited carbon formation, the anode conductivity and catalytic activity remained relatively constant, resulting in stable cell performance in dry CH_4. Further observations regarding the carbon formation in the $Cu_{1-x}Pd_x$-impregnated anodes after testing in CH_4 are provided in the next section.

3.5. Carbon formation in the $Cu_{1-x}Pd_x$-impregnated anodes

Fig. 10 shows the SEM cross-sectional images of the different $Cu_{1-x}Pd_x$-impregnated anodes in the cells which were manually fractured after the completion of the stability test in CH_4. The cross-sectional microstructural features of the $Cu_{0.6}Pd_{0.4}$-, $Cu_{0.5}Pd_{0.5}$- and $Cu_{0.25}Pd_{0.75}$-impregnated anodes are shown in Fig. 10(a)–(c), where no carbon deposits were detected. For the Pd-impregnated anode, while no visible carbon deposition was observed on the tested cell, carbon formation inside the anode was verified by

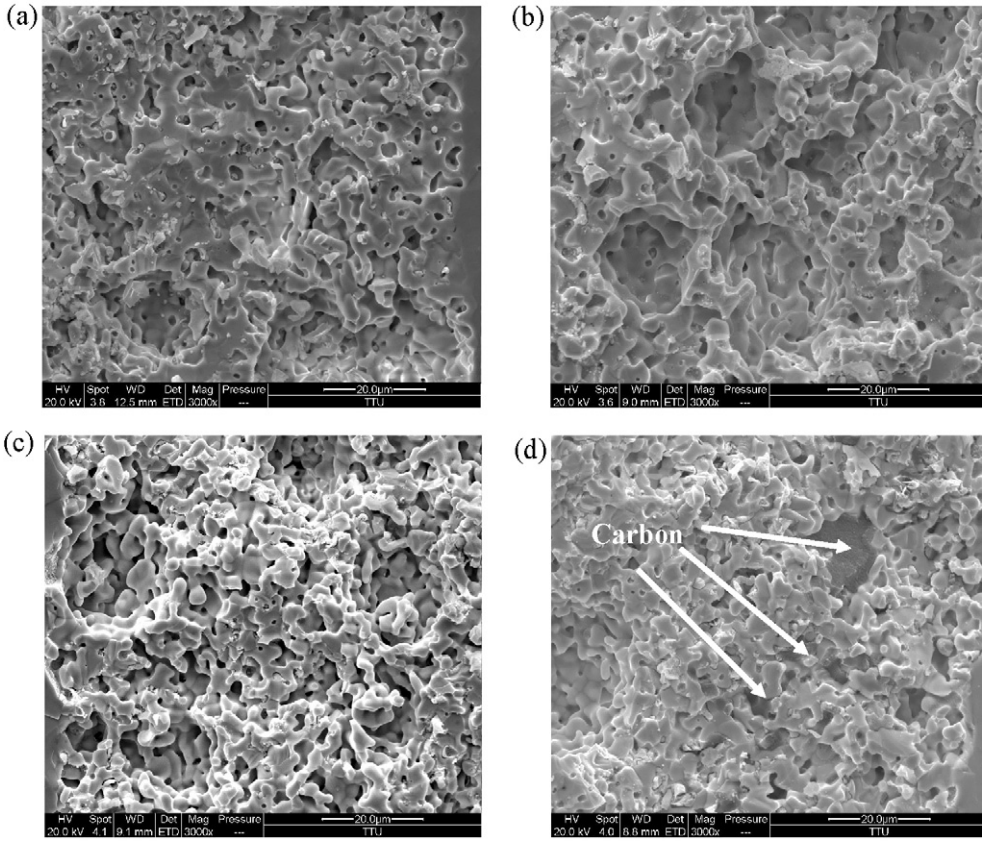

Fig. 10. SEM images of the different $Cu_{1-x}Pd_x$ alloy-impregnated anodes in the cells fractured after testing in dry CH_4 for 80 h: (a) $Cu_{0.6}Pd_{0.4}$, (b) $Cu_{0.5}Pd_{0.5}$, (c) $Cu_{0.25}Pd_{0.75}$ and (d) $Cu_0Pd_{1.0}$.

SEM/EDS. According to Fig. 10(d), the carbon deposits filled some pores in this anode, probably leading to the performance of the single cell increasing at the beginning, then dropping rapidly as the carbon blocked the pores. In addition, some areas were clean and no carbon was observed at all, possibly where no Pd impregnation occurred, due to the relatively dense structure of the porous LDC layer and low Pd loading.

Although carbon was present in the Pd-impregnated anode, the single cell was not damaged or failed during testing, likely due to the fact that no carbon fibers were formed in the anode. Furthermore, those clean areas led to a stable output power being attained after the single cell was operated with CH_4 for around 40 h. The absence of the carbon fibers in the Pt–CeO_2–LDC anode could be associated with the CeO_2 particles and the LDC support present in the anode, similar to the Pd–Ni/Ce(Sm)O_2 and Pd-Ni/La(Sr)CrO_3 catalyst systems [30–34]. After Cu was introduced to form the $Cu_{1-x}Pd_x$ alloys, no carbon deposits were observed, likely due to the Cu enrichment on the alloy surface, as mentioned earlier.

The experimental results indicate that the performance of the SOFC anodes impregnated with the Cu–Pd alloys improved significantly compared to that impregnated with Cu, while carbon deposition on the Cu–Pd alloy-containing anodes was greatly suppressed compared to the Pd-containing ones. Therefore, these Cu–Pd alloy-impregnated anodes deserve further investigation and optimization for potential direct utilization of dry methane.

4. Conclusions

$Cu_{1-x}Pd_x$ alloy-impregnated anodes have been identified for direct utilization of dry methane in the temperature range of 700–800 °C for the LSGM electrolyte-supported single cell with a co-fired porous LDC skeleton. The $Cu_{1-x}Pd_x$-impregnated (x = 0.15, 0.25, 0.4, 0.5 and 0.75) anodes showed improved performance both in dry H_2 and CH_4 compared to pure Cu-impregnated anode and also exhibited reduced carbon formation in dry CH_4 compared to a pure Pd-impregnated anode. Especially in dry CH_4, the performance of the single cells with the $Cu_{1-x}Pd_x$-impregnated anodes improved steadily with the increase in Pd content. Based on the stability testing data of the cells with the $Cu_{0.5}Pd_{0.5}$-, $Cu_{0.25}Pd_{0.75}$- and Pd-impregnated anodes, the alloying of Cu with Pd is a very effective method for increasing the overall performance stability of the single cell in dry CH_4.

Acknowledgement

This work was supported by the U.S. Army Communications-Electronics Research, Development and Engineering Center (CERDEC) under contract number W909MY-06-C-0040.

References

[1] S. Park, J.M. Vohs, R.J. Gorte, Nature 404 (2000) 265–267.
[2] S.W. Tao, J.T.S. Irvine, J. Electrochem. Soc. 151 (2004) A252–A259.
[3] Y.H. Huang, R.I. Dass, Z.L. Xing, J.B. Goodenough, Science 312 (2006) 254–257.
[4] H. Kim, J.M. Vohs, R.J. Gorte, Chem. Commun. 22 (2001) 2334–2335.
[5] H.P. He, R.J. Gorte, J.M. Vohs, Electrochem. Solid-State Lett. 8 (6) (2005) A279–A280.
[6] Z.H. Bi, J.H. Zhu, Electrochem. Solid-State Lett. 12 (2009) B107–B111.
[7] Z.F. Zhou, C. Gallo, M.B. Pague, H. Schobert, S.N. Lvov, J. Power Sources 133 (2004) 181–187.
[8] Z.F. Zhou, R. Kumar, S.T. Thakur, L.R. Rudnick, H. Schobert, S.N. Lvov, J. Power Sources 171 (2007) 856–860.
[9] M.D. Gross, J.M. Vohs, R.J. Gorte, Electrochem. Solid-State Lett. 10 (2007) B65–B69.
[10] G. Kim, G. Corre, J.T.S. Irvine, J.M. Vohs, R.J. Gorte, Electrochem. Solid-State Lett. 11 (2008) B16–B19.
[11] S.I. Lee, J.M. Vohs, R.J. Gorte, J. Electrochem. Soc. 151 (2004) A1319–A1323.

[12] H. Kim, C. Lu, W.L. Worrell, J.M. Vohs, R.J. Gorte, J. Electrochem. Soc. 149 (2002) A247–A250.
[13] A. Sin, E. Kopnin, Y. Dubitsky, A. Zaopo, A.S. Arico, D.L. Rosa, l.R. Gullo, V. Antonucci, J. Power Sources 164 (2007) 300–305.
[14] Z. Xie, C. Xia, M. Zhang, W. Zhu, H. Wang, J. Power Sources 161 (2006) 1056–1061.
[15] G.M. Grgicak, M.M. Pakulska, J.S. Obrien, J.B. Giorgi, J. Power Sources 183 (2008) 26–33.
[16] O. Costa-Nunes, J.M. Vohs, R.J. Gorte, J. Electrochem. Soc. 150 (2003) A858–A863.
[17] X.C. Lu, J.H. Zhu, Solid State Ionics 178 (2007) 1467–1475.
[18] S. McIntosh, J.M. Vohs, R.J. Gorte, Electrochem. Solid-State Lett. 6 (2003) A240–A243.
[19] S. An, C. Lu, W.L. Worrell, R.J. Gorte, J.M. Vohs, Solid State Ionics 175 (2004) 135–138.
[20] P.R. Subramanian, D.E. Laughlin, J. Phase Equil. 12 (1991) 231–236.
[21] M.D. Gross, J.M. Vohs, R.J. Gorte, J. Electrochem. Soc. 154 (2007) B694–B699.
[22] D. Ciuparu, M.R. Lyubovsky, E. Altman, L.D. Pfefferle, A. Datye, Catal. Rev. 44 (2002) 593–649.
[23] P. Gelin, M. Primet, Appl. Catal. B: Environ. 39 (2002) 1–37.
[24] E.S. Putna, J. Stubenrauch, J.M. Vohs, R.J. Grote, Langmuir 11 (1995) 4832–4837.
[25] Y.M. Ye, T.M. He, Y.B. Li, E.H. Tang, T.L. Reitz, S.P. Jiang, J. Electrochem. Soc. 155 (2008) B811–B818.
[26] B.C.H. Steele, Solid State Ionics 129 (2000) 95–110.
[27] H. Inaba, H. Tagawa, Solid State Ionics 83 (1996) 1–16.
[28] S. McIntosh, J.M. Vohs, R.J. Gorte, J. Electrochem. Soc. 150 (2003) A470–A476.
[29] A. Atkinson, S. Barnett, R.J. Gorte, J.T.S. Irvine, A.J. McEvoy, M. Mogensen, S.C. Singhal, J. Vohs, Nat. Mater. 3 (2004) 17–27.
[30] Y. Nabae, I. Yamanaka, M. Hatano, K. Otsuka, J. Electrochem. Soc. 153 (2006) A140–A145.
[31] Y. Nabae, I. Yamanaka, M. Hatano, K. Otsuka, J. Phys. Chem. C 112 (2008) 10308–10315.
[32] R.T.K. Baker, Carbon 27 (1989) 315–323.
[33] S. Takenaka, Y. Shigeta, E. Tanabe, K. Otsuka, J. Phys. Chem. B 108 (2004) 7656–7664.
[34] L. Kepinski, Catal. Today 50 (1999) 237–245.